Supplemental Material for Topology of Disconnected Elementary Band Representations

Jennifer Cano,[1] Barry Bradlyn,[1] Zhijun Wang,[2] L. Elcoro,[3] M. G. Vergniory,[4,5,6] C. Felser,[7] M. I. Aroyo,[3] and B. Andrei Bernevig[2,4,8,9,10,*]

[1] *Princeton Center for Theoretical Science, Princeton University, Princeton, New Jersey 08544, USA*
[2] *Department of Physics, Princeton University, Princeton, New Jersey 08544, USA*
[3] *Department of Condensed Matter Physics, University of the Basque Country UPV/EHU, Apartado 644, 48080 Bilbao, Spain*
[4] *Donostia International Physics Center, P. Manuel de Lardizabal 4, 20018 Donostia-San Sebastián, Spain*
[5] *Department of Applied Physics II, University of the Basque Country UPV/EHU, Apartado 644, 48080 Bilbao, Spain*
[6] *Ikerbasque, Basque Foundation for Science, 48013 Bilbao, Spain*
[7] *Max Planck Institute for Chemical Physics of Solids, 01187 Dresden, Germany*
[8] *Laboratoire Pierre Aigrain, Ecole Normale Supérieure-PSL Research University, CNRS, Université Pierre et Marie Curie-Sorbonne Universités, Université Paris Diderot-Sorbonne Paris Cité, 24 rue Lhomond, 75231 Paris Cedex 05, France*
[9] *Sorbonne Universités, UPMC Univ Paris 06, UMR 7589, LPTHE, F-75005, Paris, France*
[10] *LPTMS, CNRS (UMR 8626), Université Paris-Saclay, 15 rue Georges Clémenceau, 91405 Orsay, France*

S1. NEAREST NEIGHBOR HAMILTONIAN FOR $p_{x,y}$ ORBITALS ON THE HONEYCOMB LATTICE

We choose the lattice basis vectors:

$$\begin{aligned}\mathbf{e}_1 &= \frac{\sqrt{3}}{2}\hat{\mathbf{x}} + \frac{1}{2}\hat{\mathbf{y}}\\ \mathbf{e}_2 &= \frac{\sqrt{3}}{2}\hat{\mathbf{x}} - \frac{1}{2}\hat{\mathbf{y}},\end{aligned} \tag{S1}$$

which are shown in Fig. 1 with their reciprocal lattice vectors, $\mathbf{g}_i$, which satisfy $\mathbf{g}_i \cdot \mathbf{e}_j = 2\pi\delta_{ij}$. Sites on the $A(B)$ sublattice sit at positions $\mathbf{R} + \mathbf{r}_{A(B)}$, where $\mathbf{R}$ denotes a lattice translation and

$$\begin{aligned}\mathbf{r}_A &= \frac{2}{3}\mathbf{e}_1 - \frac{1}{3}\mathbf{e}_2\\ \mathbf{r}_B &= \frac{1}{3}\mathbf{e}_1 - \frac{2}{3}\mathbf{e}_2\end{aligned} \tag{S2}$$

In this basis, the symmetry generators of the honeycomb lattice act as follows:

$$\begin{aligned}C_{3z} &: (\mathbf{e}_1, \mathbf{e}_2) \to (-\mathbf{e}_2, \mathbf{e}_1 - \mathbf{e}_2)\\ C_{2z} &: (\mathbf{e}_1, \mathbf{e}_2) \to (-\mathbf{e}_1, -\mathbf{e}_2)\\ m_{1\bar{1}} &: (\mathbf{e}_1, \mathbf{e}_2) \to (\mathbf{e}_2, \mathbf{e}_1),\end{aligned} \tag{S3}$$

where the subscript $1\bar{1}$ indicates that the mirror plane has normal vector $\mathbf{e}_1 - \mathbf{e}_2$. For $p_{x,y}$ orbitals, we choose the following matrix representation, in which the Pauli matrices τ act in sublattice space and the σ matrices act in orbital space:

$$\begin{aligned}U_{C_{3z}} &= \tau_0 \otimes \left(-\frac{1}{2}\sigma_0 + i\frac{\sqrt{3}}{2}\sigma_y\right)\\ U_{C_{2z}} &= -\tau_x \otimes \sigma_0\\ U_{m_{1\bar{1}}} &= \tau_0 \otimes \sigma_z,\end{aligned} \tag{S4}$$

The orbital term for a rotation by an angle θ about an axis $\hat{\mathbf{n}}$ is represented by $e^{i\theta\hat{\mathbf{n}}\cdot\mathbf{S}}$, projected onto the $p_{x,y}$ orbitals; $\mathbf{S}$ is the vector of spin-1 matrices. A Hamiltonian, $H_{\mathbf{k}}$, that respects the lattice symmetry must satisfy:

$$H_{\mathbf{k}} = U_R^\dagger H_{R\mathbf{k}} U_R, \tag{S5}$$

for each generator, R, of the honeycomb lattice.

Denoting the annihilation operator on site $\mathbf{r}$ by $c_{\mathbf{r},a}$, where $a = x, y$ indicates the p_x or p_y orbital, the nearest neighbor Hamiltonian is given by:

$$H = \sum_{\mathbf{R}}\sum_{a,b}\sum_{\delta_i} t_{ab}(\delta_i) c^\dagger_{\mathbf{R}+\mathbf{r}_A,a} c_{\mathbf{R}+\mathbf{r}_A+\delta_i,b} + \text{h.c.}, \tag{S6}$$

where the three nearest neighbors to a site at $\mathbf{R}+\mathbf{r}_A$ sit at $\mathbf{R}+\mathbf{r}_A+\delta_i$ (the vectors δ_i are depicted in Fig. 1) and $t_{ab}(\delta_i)$ is given by one of the Slater-Koster terms:[1]

$$\begin{aligned}t_{xx}(\delta_i) &= \frac{1}{3}\left[(\delta_i\cdot\hat{\mathbf{x}})^2 t_\sigma + (\delta_i\cdot\hat{\mathbf{y}})^2 t_\pi\right]\\ t_{yy}(\delta_i) &= \frac{1}{3}\left[(\delta_i\cdot\hat{\mathbf{y}})^2 t_\sigma + (\delta_i\cdot\hat{\mathbf{x}})^2 t_\pi\right]\\ t_{xy}(\delta_i) &= \frac{1}{3}(\delta_i\cdot\hat{\mathbf{x}})(\delta_i\cdot\hat{\mathbf{y}})(t_\sigma - t_\pi) = t_{yx}(\delta_i),\end{aligned} \tag{S7}$$

where $t_{\sigma(\pi)}$ are free parameters that describe $\sigma(\pi)$-bonds. Notice that $\mathbf{r}_A + \delta_i$ is always a site on the B sublattice. Using the Fourier transform,

$$c_{\mathbf{k},L,a} = \sum_{\mathbf{R}} e^{i\mathbf{k}\cdot(\mathbf{R}+\mathbf{r}_L)} c_{\mathbf{R}+\mathbf{r}_L,a} \tag{S8}$$

where $L = A, B$ denotes the sublattice and $a = x, y$ denotes the orbital, the real space Hamiltonian in Eq (S6) is rewritten:

$$H = \sum_{\mathbf{k}}\sum_{a,b}\sum_{\delta_i} c^\dagger_{\mathbf{k},A,a} c_{\mathbf{k},B,b} e^{-i\mathbf{k}\cdot\delta_i} t_{ab}(\delta_i) + \text{h.c.}, \tag{S9}$$

Plugging Eq (S7) into Eq (S9) yields

$$H^0 = \sum_{\mathbf{k}} \psi^\dagger_{\mathbf{k}} H^0_{\mathbf{k}} \psi_{\mathbf{k}} \equiv \sum_{\mathbf{k}} \psi^\dagger_{\mathbf{k}} \begin{pmatrix} 0 & h_{\mathbf{k}} \\ h^\dagger_{\mathbf{k}} & 0 \end{pmatrix} \psi_{\mathbf{k}} \tag{S10}$$

where $\psi_{\mathbf{k}} = \begin{pmatrix} c_{\mathbf{k},A,x} & c_{\mathbf{k},A,y} & c_{\mathbf{k},B,x} & c_{\mathbf{k},B,y} \end{pmatrix}^T$ contains the annihilation operators for $p_{x,y}$ orbitals on the A and B sublattices and $h_{\mathbf{k}}$ is given by Eq. (3).

A. Phase diagram of $H^0_{\mathbf{k}} + xH^1_{\mathbf{k}}$

As described in the main text, a necessary condition to reach the gapped TCI phase is that the two-fold degeneracy at K is higher or lower in energy than the other two bands. The eigenvalues of $H^0_{\mathbf{k}=K} + xH^1_{\mathbf{k}=K}$ are $-\frac{3\sqrt{3}}{8}x$ (2-fold degenerate) and $\frac{3}{8}(\pm 4(t_\pi - t_\sigma) + \sqrt{3}x)$; thus, the TCI phase requires:

$$|x| > \frac{2}{\sqrt{3}}|t_\pi - t_\sigma| \tag{S11}$$

However, there are further constraints: band crossings along the paths connecting Γ and M can prevent the system from opening a gap even when the energy ordering at K allows it. Consider the two lines $\Sigma = \alpha \mathbf{g}_1$ and $\Lambda = \beta(\frac{1}{3}\mathbf{g}_1 + \frac{2}{3}\mathbf{g}_2)$, which are invariant under $C_{3z}m_{1\bar{1}}$ and $C_{2z}C_{3z}m_{1\bar{1}}$, respectively. As α goes from 0 to $\frac{1}{2}$, Σ connects Γ to M. As β goes from 0 to $\frac{3}{2}$, Λ connects Γ to $M+\mathbf{g}_2$ (passing through K' at $\beta = 1$). We can then track the respective mirror eigenvalues along these lines to find constraints on connectivity. The BANDREP application on the BCS server shows that the Γ_5 and Γ_6 irreps appear at Γ in our model ($p_{x,y}$ orbitals on the honeycomb correspond to the irrep E at Wyckoff position $2b$). In the Γ_5 and Γ_6 irreps, the character of each mirror is zero: this means that the doubly-degenerate bands that comprise the Γ_5 irrep will split into two bands along Σ, one of which is even under $C_{3z}m_{1\bar{1}}$ and one of which is odd (and same for Γ_6). Thus, Γ_5 must connect to two irreps at M which have opposite parity under $C_{3z}m_{1\bar{1}}$. Similarly, the Γ_5 irrep will split into two bands along Λ, one of which is even under $C_{2z}C_{3z}m_{1\bar{1}}$ and one of which is odd; thus, Γ_5 must connect to two irreps at M which have opposite parity under $C_{2z}C_{3z}m_{1\bar{1}}$. Without loss of generality, assume the Γ_5 irrep is higher in energy than Γ_6; then in order for the system to be an insulator, the two bands that are highest in energy at M must have opposite $C_{3z}m_{1\bar{1}}$ eigenvalues and also opposite $C_{2z}C_{3z}m_{1\bar{1}}$ eigenvalues.

Referring to Table S1, a gapped band structure requires one of the two following conditions to be satisfied:

$$E_{M1,M2} > E_{M3,M4} \Rightarrow 3t_\sigma < t_\pi < \frac{1}{3}t_\sigma \tag{S12}$$

$$E_{M1,M2} < E_{M3,M4} \Rightarrow \frac{1}{3}t_\pi < t_\sigma < 3t_\pi \tag{S13}$$

If neither Eq (S12) or (S13) is satisfied, there will be a band crossing along $\Gamma - M$, as shown in Fig S1a.

The C_{2z} eigenvalues at Γ are shown in Table S2. By comparing Table S1 with Table S2, one can check that in the gapped phase, when either Eq (S12) or (S13) is satisfied, the C_{2z} eigenvalues at Γ are always opposite those at M (unlike the usual time-reversal $\mathbb{Z}_2$ invariant, here we are referring to the C_{2z} eigenvalues themselves, not their product. This guarantees that the Wilson loop in Fig. 1d always winds in the gapped phase.[2]

We note that it could be possible with longer range hopping terms to reach a gapped phase where the C_{2z} eigenvalues of the two lower bands at Γ are the same as those at M (this is symmetry-allowed according to possible decompositions of the EBR induced from $p_{x,y}$ orbitals listed on the BCS Server[3]). However, this phase is not accessible within our nearest-neighbor model.

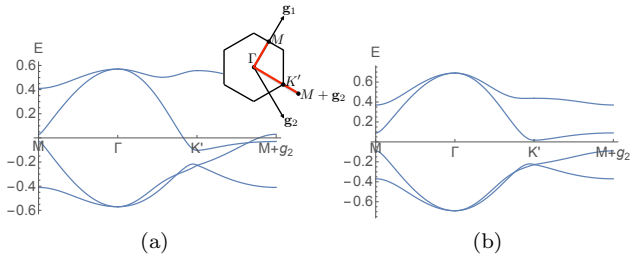

FIG. S1. Band structure of $H^0_{\mathbf{k}} + xH^1_{\mathbf{k}}$ along the red path shown in the inset; $x = .35$. In (a) $t_\sigma = .08, t_\pi = .3$, while in (b) $t_\sigma = .16, t_\pi = .3$. In both cases, Eq (S11) is satisfied; hence the band ordering at K allows for a gap. However, since the parameters in (a) violate Eq (S12) and (S13), there is a band crossing between Γ and $M + \mathbf{g}_2$. In (b), Eq (S13) is satisfied and the band structure is gapped.

Energy at M	$C_{3z}m_{1\bar{1}}$ eig.	$C_{2z}C_{3z}m_{1\bar{1}}$ eig.	C_{2z} eig.
$E_{M1} \equiv \frac{t_\pi}{2} - \frac{3t_\sigma}{2}$	-1	1	-1
$E_{M2} \equiv -\frac{3t_\pi}{2} + \frac{t_\sigma}{2}$	1	-1	-1
$E_{M3} \equiv \frac{3t_\pi}{2} - \frac{t_\sigma}{2}$	1	1	$+1$
$E_{M4} \equiv -\frac{t_\pi}{2} + \frac{3t_\sigma}{2}$	-1	-1	$+1$

TABLE S1. Energies, mirror, and C_{2z} eigenvalues for each of the eigenstates at M. The C_{2z} eigenvalue is a product of the two mirror eigenvalues.

Energy at Γ	C_{2z} eig.
$E_{\Gamma 1} = -\frac{3}{2}(t_\pi + t_\sigma)$	$+1, +1$
$E_{\Gamma 2} = \frac{3}{2}(t_\pi + t_\sigma)$	$-1, -1$

TABLE S2. Energies and C_{2z} eigenvalues for the two-fold degenerate eigenstates at Γ.

B. Irreps at high-symmetry points

Using the notation on BANDREP application of the BCS[3], the Hamiltonian $H^0_{\mathbf{k}} + xH^1_{\mathbf{k}}$ can realize two possible sets of valence bands: $(\Gamma_5, K_3, M_3, M_4)$ or $(\Gamma_6, K_3, M_1, M_2)$, assuming, without loss of generality, that the K_3 irrep appears in the valence bands instead of the conduction bands. (As noted at the end of the last section, there are two other disconnected phases listed in the BANDREP application that that our model does not realize and which differ in the C_{2z} eigenvalues of occupied bands; presumably they require longer range hopping). By comparing to the list of band representations induced from Wyckoff positions in $P6mm$ (SG 183) (which describes layers of the honeycomb lattice with no additional symmetry in the z direction), we see that the irreps in $A_1 \uparrow G$ or $B_2 \uparrow G$ from the $1a$ position are (Γ_1, K_1, M_1) or (Γ_3, K_1, M_3), respectively, while the irreps in $A_1 \uparrow G$ on the $3c$ position are $(\Gamma_1, \Gamma_5, K_1, K_3, M_1, M_3, M_4)$ and the irreps in $B_1 \uparrow G$ on the $3c$ position are $(\Gamma_3, \Gamma_6, K_1, K_3, M_1, M_2, M_3)$. Thus, we see that for each of the possible sets of valence bands in our model, the irreps that appear are obtained from subtracting the irreps of one of the EBRs induced from the $1a$ position from one of the EBRs induced from the $3c$ position. A classification scheme that only looks at the irreps at high-symmetry points will classify our valence bands as trivial. It was noted in Ref 4 that some topologically nontrivial bands will be included in the trivial class; our model is an example of this phenomenon.

C. Phase diagram with SOC

Including SOC, $\Gamma_5 \to \bar{\Gamma}_7 \oplus \bar{\Gamma}_8$, $\Gamma_6 \to \bar{\Gamma}_7 \oplus \bar{\Gamma}_9$ and $K_1 \to \bar{K}_6$, $K_2 \to \bar{K}_6$, $K_3 \to \bar{K}_4 \oplus \bar{K}_5 \oplus \bar{K}_6$. Thus, the irreps that appear in a model with spinful $p_{x,y}$ orbitals on the honeycomb lattice are

$$2\bar{\Gamma}_7 \oplus \bar{\Gamma}_8 \oplus \bar{\Gamma}_9 \text{ and } 3\bar{K}_6 \oplus \bar{K}_4 \oplus \bar{K}_5 \tag{S14}$$

As mentioned in the main text, they belong to a sum of three EBRs, ${}^1\bar{E} \uparrow G$, ${}^2\bar{E} \uparrow G$, and $\bar{E}_1 \uparrow G$, induced from the $2b$ position. The double-valued EBRs for SG 183 are listed in Table S3. (Since there is only one double-valued irrep of the little group at M, it cannot be used to distinguish EBRs and we do not need to consider it here.) Since the $\bar{E}_1 \uparrow G$ EBR is decomposable, generically, the band structure splits into four groups of bands. One possibility is that one branch contains the irreps $\bar{\Gamma}_8$ and $\bar{K}_6$, another contains $\bar{\Gamma}_9$ and $\bar{K}_6$, another contains $\bar{\Gamma}_7$ and $\bar{K}_6$ and the last contains $\bar{\Gamma}_7$ and $\bar{K}_4 \oplus \bar{K}_5$. In this case, each branch has the same irreps at high-symmetry points as an EBR listed in Table S3, but the EBR might come from orbitals on the $1a$ position. In the language of Ref 5, a branch that contains the same irreps as an EBR induced from orbitals located at a different site than the atoms is called an "obstructed atomic limit." An obstructed atomic limit can have localized Wannier functions, but since those Wannier functions are not located where the atoms are located, a gap must close in order to reach the phase where the Wannier functions and the atomic orbitals are localized at the same sites.

The other possibility is that the bands disconnect in such a way that some branches do not have the same irreps as an EBR; this can happen if a branch contains $\bar{\Gamma}_8$ or $\bar{\Gamma}_9$ and $\bar{K}_4 \oplus \bar{K}_5$. A branch that does not have the same irreps as an EBR does not correspond to an atomic limit and cannot yield maximally localized Wannier functions that obey the crystal symmetry, centered at any position.

Wyckoff	EBR	$\bar{\Gamma}$ irreps	$\bar{K}$ irreps	No. bands
$1a$	$\bar{E}_1 \uparrow G$	$\bar{\Gamma}_9$	$\bar{K}_6$	2
$1a$	$\bar{E}_2 \uparrow G$	$\bar{\Gamma}_8$	$\bar{K}_6$	2
$1a$	$\bar{E}_3 \uparrow G$	$\bar{\Gamma}_7$	$\bar{K}_4 \oplus \bar{K}_5$	2
$2b$	${}^1\bar{E} \uparrow G$	$\bar{\Gamma}_7$	$\bar{K}_6$	2
$2b$	${}^2\bar{E} \uparrow G$	$\bar{\Gamma}_7$	$\bar{K}_6$	2
$2b$	$\bar{E}_1 \uparrow G$	$\bar{\Gamma}_8 \oplus \bar{\Gamma}_9$	$\bar{K}_4 \oplus \bar{K}_5 \oplus \bar{K}_6$	4

TABLE S3. Double-valued EBRs in SG 183, obtained from the BANDREP application.[3]

When time-reversal symmetry is imposed, we can compute the $\mathbb{Z}_2$ index. Let us first consider the case when SOC is spin-conserving; following Ref 5, we refer to this as "Haldane" SOC, as opposed to Rashba SOC, which, by our definition, is any SOC term that does not conserve spin. An SOC term that conserves spin will also preserve inversion symmetry (the inversion operator is exactly the tensor product of the spinless C_{2z} operator in Eq (S4) and the identity in spin space). We can compute the $\mathbb{Z}_2$ index[6] from the product of C_{2z} eigenvalues at Γ and M, since each band in the spinless model gives rise to a Kramers pair with SOC, whose inversion eigenvalue is the same as the spinless C_{2z} eigenvalue. The eigenvalues of C_{2z} are given in Tables S1 and S2 and the product for each band is tabulated in Table S4 for all parameter regimes. (Note: there are three inequivalent M points, but they share the same C_{2z} eigenvalues). The ordered lists of C_{2z} eigenvalues in the last column of Table S4 reflect the particle-hole symmetry of our simplistic model; however, terms that break the particle-hole symmetry without inverting bands at Γ or M will not change the order of eigenvalues. The fact that some particle-hole symmetric arrangements do not appear (namely, $+1, +1, +1, +1$ and $+1, -1, -1, +1$, is a surprising feature of our simple model.) Since the product of C_{2z} eigenvalues of the lowest band is always -1, whenever SOC opens a gap to the lowest energy band, it is a topological gap. If there is a gap at half-filling, there are two possibilities: if the gap was open before SOC was added, then the parameters $t_{\sigma,\pi}$ are constrained by Eqs (S12)–(S13); comparing to Table S4 reveals that this gap will have a trivial $\mathbb{Z}_2$ index (consistent with the fact that a spinless model must have a trivial $\mathbb{Z}_2$ index.) On the other hand, in the parameter regime that violates

Eqs (S12)–(S13), the spinless system will be gapless at half-filling; if SOC opens a gap, then Table S4 shows that the gap has a nontrivial $\mathbb{Z}_2$ index.

We now consider non-spin-conserving (Rashba) SOC and examine each of the high-symmetry points. First, Rashba SOC cannot open a gap at M since each spinless band is non-degenerate (when SOC is turned on, it will become a Kramers pair.) Second, Rashba SOC cannot open a gap at K: if two bands are degenerate at K in the spinless model, then they are in the K_3 representation, which we showed in the supplement of Ref 5 (Sec IIID) can only be gapped if the strength of Haldane SOC exceeds that of Rashba SOC. Third, we examine the Γ point. In the spinless model, bands come in degenerate pairs, which are described by the Γ_5 or Γ_6 representation, where C_{2z} is represented by $\pm\mathbb{I}$. When we consider spin, C_{2z} is represented by $\pm\mathbb{I}\otimes is_z$, where s_z is the Pauli matrix describing the spin degrees of freedom. A term that breaks spin conservation will not commute with $\mathbb{I}\otimes is_z$. Hence, no Rashba term can appear at the Γ point because it will break C_{2z} symmetry. We conclude from examining all three high-symmetry points that any gap that is opened by small SOC is adiabatically related to a gap that is opened by spin-conserving SOC and hence the $\mathbb{Z}_2$ topological index obtained from inversion eigenvalues still holds.

Parameter regime	Prod. C_{2z} eigs.
$t_\pi < -t_\sigma$, $t_\pi < 3t_\sigma$ $\Rightarrow$ $E_{\Gamma 2} < E_{\Gamma 1}$, $E_{M3} < E_{M1} < E_{M4} < E_{M2}$	$-1,+1,+1,-1$
$t_\pi > 3t_\sigma$, $t_\pi < \frac{1}{3}t_\sigma$ $\Rightarrow$ $E_{\Gamma 2} < E_{\Gamma 1}$, $E_{M3,M4} < E_{M1,M2}$	$-1,-1,-1,-1$
$t_\pi < -t_\sigma$, $t_\pi > \frac{1}{3}t_\sigma$ $\Rightarrow$ $E_{\Gamma 2} < E_{\Gamma 1}$, $E_{M4} < E_{M2} < E_{M3} < E_{M1}$	$-1,+1,+1,-1$
$t_\pi > -t_\sigma$, $t_\pi > 3t_\sigma$ $\Rightarrow$ $E_{\Gamma 1} < E_{\Gamma 2}$, $E_{M2} < E_{M4} < E_{M1} < E_{M3}$	$-1,+1,+1,-1$
$t_\pi > \frac{1}{3}t_\sigma$, $t_\pi < 3t_\sigma$ $\Rightarrow$ $E_{\Gamma 1} < E_{\Gamma 2}$, $E_{M1,M2} < E_{M3,M4}$	$-1,-1,-1,-1$
$t_\pi > -t_\sigma$, $t_\pi < \frac{1}{3}t_\sigma$ $\Rightarrow$ $E_{\Gamma 1} < E_{\Gamma 2}$, $E_{M1} < E_{M3} < E_{M2} < E_{M4}$	$-1,+1,+1,-1$

TABLE S4. Product of C_{2z} eigenvalues at Γ and M in order of increasing energy, for all possible parameter regimes. According to Eqs (S12) and (S13), the spinless model can only be gapped in the parameter regimes corresponding to the second or fifth row.

S2. d_{z^2} AND $d_{x^2-y^2}$ ORBITALS IN $P4_232$

Since the lattice of $P4_232$ (SG 208) is primitive cubic, the lattice vectors are $\mathbf{e}_1 = \hat{\mathbf{x}}, \mathbf{e}_2 = \hat{\mathbf{y}}, \mathbf{e}_3 = \hat{\mathbf{z}}$. A unit cell is drawn in Fig. 3a; we take the origin to be one of the corners of the cube. Our model consists of d_{z^2} and $d_{x^2-y^2}$ orbitals sitting at the corners and center of the cube. These orbitals transform as representations of T (generated by C_{2z} and $C_{3,111}$), which is the "site-symmetry group" of the origin:[7] that is, T is the largest subset of $P4_232$ that leaves the origin invariant. The d_{z^2} and $d_{x^2-y^2}$ orbitals transform as the one-dimensional irreps, ${}^1E$ and ${}^2E$, of T.[8] Since they are time-reversed partners, they transform as a single irrep under the symmetries of T and time-reversal. (We also note that the tensor product of the spin-$\frac{1}{2}$ representation with d_{z^2} and $d_{x^2-y^2}$ orbitals yields the two-dimensional irreps, ${}^1F_{3/2}$ and ${}^2F_{3/2}$.[9]) Instead of choosing the diagonal set of matrix representatives, we choose a physically motivated basis, where a rotation by an angle θ about an axis $\hat{\mathbf{n}}$ is represented by $e^{i\theta\hat{\mathbf{n}}\cdot\mathbf{S}}$, projected onto the d_{z^2} and $d_{x^2-y^2}$ orbitals. This yields $C_{2z} = C_{2x} = C_{2y} = \sigma_0$, and

$$C_{3,111} = -\frac{1}{2}\mathbb{I} + \frac{\sqrt{3}}{2}(i\sigma_y) = \begin{pmatrix} -\frac{1}{2} & \frac{\sqrt{3}}{2} \\ -\frac{\sqrt{3}}{2} & -\frac{1}{2} \end{pmatrix} \tag{S15}$$

The screw operation $\tilde{C}_{2,110} \equiv \{C_{2,110}|\frac{1}{2}\frac{1}{2}\frac{1}{2}\}$ mixes the two sublattices consisting of sites at the origin and sites at the center, $(\frac{1}{2},\frac{1}{2},\frac{1}{2})$, of each unit cell. The full representation of the symmetry operations is given by:

$$\begin{aligned} U_{C_{2z}} &= U_{C_{2y}} = \tau_0 \otimes \sigma_0 \\ U_{C_{3,111}} &= \tau_0 \otimes (-\frac{1}{2}\sigma_0 + \frac{\sqrt{3}}{2} i\sigma_y) \\ U_{\tilde{C}_{2,110},\mathbf{k}} &= e^{-\frac{i}{2}(k_x+k_y-k_z)}\tau_x \otimes \sigma_z, \end{aligned} \tag{S16}$$

where the τ matrices act in the sublattice space. Time-reversal is implemented by complex conjugation. Since the representation cannot be reduced without breaking time-reversal symmetry, it is "physically irreducible."[10]

S3. SYMMETRY CONSTRAINTS ON THE WILSON LOOP IN $P4_232$ (SG 208)

We show how the symmetries of $P4_232$ constrain the z-directed Wilson loop defined in Eq. (1); we will always take the base point $k_{z0} = 0$. We will frequently utilize the transformation of the Wilson loop under a non-symmorphic unitary symmetry, $\{D_g|(\delta_x,\delta_y,\delta_z)\}$, such that D_g acts in momentum space by $(k_\perp, k_z) \to (D_g k_\perp, -k_z)$, then

$$\mathcal{W}_{(D_g k_\perp, k_{z0})} = e^{2\pi i \delta_z} \tilde{U}_g(k_\perp, k_{z0}) \mathcal{W}^\dagger_{(k_\perp, -k_{z0})} (\tilde{U}_g(k_\perp, k_{z0}))^\dagger, \tag{S17}$$

where

$$\left[\tilde{U}_g(\mathbf{k})\right]_{nm} \equiv \langle u^n(D_g\mathbf{k})|U_g|u^m(\mathbf{k})\rangle \tag{S18}$$

This is a variation of Eq (B19) in Ref 11 or Eq (D8) in Ref 12. If D_g does not invert k_z, then there is no dagger on $\mathcal{W}$ on the right-hand side of Eq (S17).

A. Wilson eigenvalues along $\bar{\Gamma}-\bar{X}-\bar{M}-\bar{Y}-\bar{\Gamma}$

Let us first consider the eigenvalues of the Wilson matrix at $\bar{\Gamma}$. Enforcing C_{2x} symmetry, (recall, $U_{C_{2x}}=\mathbb{I}_{4\times4}$ from Eq (S16)), Eq (S18) shows that $\tilde{U}_{C_{2x}}(\Gamma)=\mathbb{I}_{2\times2}$; then Eq (S17) yields $\mathcal{W}_{(\bar{\Gamma},0)}=\mathcal{W}^{\dagger}_{(\bar{\Gamma},0)}$. This forces the eigenvalues of $\mathcal{W}_{(\bar{\Gamma},0)}$ to be real. Enforcing $\tilde{C}_{2,110}$ symmetry (which has $\delta_z=\frac{1}{2}$), Eq (S17) yields $\mathcal{W}_{(\bar{\Gamma},0)}=-\tilde{U}_{\tilde{C}_{2,110}}\mathcal{W}^{\dagger}_{(\bar{\Gamma},0)}\tilde{U}^{\dagger}_{\tilde{C}_{2,110}}$, which shows that the eigenvalues of $\mathcal{W}_{(\bar{\Gamma},0)}$ must be equal to $+1$ and -1.

Along the segment $\bar{\Gamma}-\bar{X}$, even without knowing $\tilde{U}_{C_{2x}}(\mathbf{k})$, we can utilize Eq (S17) to deduce that the eigenvalues of $\mathcal{W}_{(k_x,0,0)}$ are equal to those of $\mathcal{W}^{\dagger}_{(k_x,0,0)}$. Consequently, the eigenvalues of $\mathcal{W}_{(k_x,0,0)}$ must either come in complex conjugate pairs or be real. However, since the eigenvalues of $\mathcal{W}_{(0,0,0)}$ are $+1$ and -1, the eigenvalues of $\mathcal{W}_{(k_x,0,0)}$ must also be fixed to $+1$ and -1 along the entire line, since there is no way for them to smoothly vary while satisfying the constraints of C_{2x}.

Applying the same logic along $\bar{X}-\bar{M}$ and $\bar{Y}-\bar{\Gamma}$ with C_{2y} symmetry shows that the eigenvalues of $\mathcal{W}_{(\pi,k_y,0)}$ and $\mathcal{W}_{(0,k_y,0)}$ must also be pinned to $+1$ and -1. Finally, applying C_{2x} to $\bar{M}-\bar{Y}$ to the eigenvalues of $\mathcal{W}_{(k_x,\pi,0)}$, we deduce that the eigenvalues of the z-directed Wilson matrix are equal to $+1$ and -1 along the entire loop $\bar{\Gamma}-\bar{X}-\bar{M}-\bar{Y}-\bar{\Gamma}$.

B. Protected band crossing along $\bar{\Gamma}-\bar{M}$

Applying Eq (S17) with $\tilde{C}_{2,110}$ symmetry to the line $\bar{\Gamma}-\bar{M}$ shows that the eigenvalues of $\mathcal{W}_{(k,k,0)}$ are the same as the eigenvalues of $-\mathcal{W}^{\dagger}_{(k,k,0)}$; hence, the eigenvalues of $\mathcal{W}_{(k,k,0)}$ are either pure imaginary or come in pairs

$$\lambda(k),-\lambda(k)^* \tag{S19}$$

We showed in Sec S3 A that the eigenvalues of $\mathcal{W}_{(0,0,0)}$ (and $\mathcal{W}_{(\pi,\pi,0)}$) are $+1$ and -1; this rules out the first possibility and hence the eigenvalues of $\mathcal{W}_{(k,k,0)}$ come in pairs $(\lambda(k),-\lambda(k)^*)$, which are degenerate when $\lambda(k)=\pm i$. We now show that such a degeneracy can occur without any fine-tuning and that the parity of the number of degeneracies between $k=0$ and $k=\pi$ constitutes a topological invariant.

To see this, we rely on an anti-unitary symmetry of the Hamiltonian: $\mathcal{A}\equiv\mathcal{T}\tilde{C}^{-1}_{2,110}C_{2z}=\mathcal{T}\{C_{2,1\bar{1}0}|\frac{\bar{1}}{2}\frac{\bar{1}}{2}\frac{1}{2}\}$, satisfying $\mathcal{A}^2=1$. Since $\mathcal{A}$ leaves (k,k,k_z) invariant, the (antiunitary) generalization of Eq (S17) is:

$$\mathcal{W}_{(k,k,k_{z0})}=-\tilde{U}_A(k,k,k_{z0})K\mathcal{W}_{(k,k,k_{z0})}K(\tilde{U}_A(k,k,k_{z0}))^{\dagger}, \tag{S20}$$

where the minus sign comes from the fact that $\mathcal{A}$ includes a $\frac{1}{2}$ translation in the $\hat{z}$ direction ($e^{2\pi i\delta_z}=-1$), K is the complex conjugation operator, and

$$\left[\tilde{U}_A(\mathbf{k})\right]_{nm}\equiv\langle u^n(\mathbf{k})|\mathcal{A}|u^m(\mathbf{k})\rangle \tag{S21}$$

Notice that $(\tilde{U}_AK)^2=\mathbb{I}_{2\times2}$, from which it follows that $\tilde{U}_A(\mathbf{k})=e^{ib_0(\mathbf{k})+ib(\mathbf{k})(\cos\theta(\mathbf{k})\sigma_x+\sin\theta(\mathbf{k})\sigma_z)}$. Importantly, σ_y does not appear in the exponential. Consequently $\tilde{U}_A$ is diagonalized by $\tilde{U}_A(\mathbf{k})=e^{ib_0(\mathbf{k})}O(\mathbf{k})D(\mathbf{k})O(\mathbf{k})^T$, where $O(\mathbf{k})$ is a real orthogonal matrix and $D(\mathbf{k})=\mathrm{Diag}[e^{-ib(\mathbf{k})},e^{ib(\mathbf{k})}]$. Defining

$$W_k=O(k,k,0)^T\mathcal{W}_{(k,k,0)}O(k,k,0), \tag{S22}$$

Eq (S20) yields

$$W_k=-D(k,k,0)W_k^*D(k,k,0)^* \tag{S23}$$

Since W_k has the same eigenvalues as $\mathcal{W}_{(k,k,0)}$, whose eigenvalues must come in pairs given by Eq (S19), W_k can be written as

$$W_k=ie^{i\mathbf{a}(k)\cdot\sigma} \tag{S24}$$

for a smooth vector function $\mathbf{a}(k)=(a_x(k),a_y(k),a_z(k))$. Eq (S23) then places the following constraints at each $\mathbf{k}$:

$$a_z\sin|\mathbf{a}|=0=(a_y\sin b+a_x\cos b)\cos|\mathbf{a}| \tag{S25}$$

Since $\mathbf{a}(k)$ is a smoothly varying function, there are two possibilities: either $\cos|\mathbf{a}(k)|=0$ for all k (in which case the eigenvalues of W_k are fixed to ±1) or $\sin|\mathbf{a}(k)|\neq0$, $\cos|\mathbf{a}(k)|\neq0$ except at isolated points, in which case, $a_x(k)\propto a_y(k),a_z(k)=0$. (We rule out the case where $\sin|\mathbf{a}(k)|=0$ for all k because it is inconsistent with the fact that the eigenvalues of $W_{k=0}$ are equal to ±1.) The condition $a_x(k)\propto a_y(k),a_z(k)=0$ means that degeneracies in the spectrum of W_k (and hence $\mathcal{W}_{(k,k,0)}$) occur when $a_x(k)=0$, which forces $a_y(k)=0$. If such a degeneracy is present and linear in k, then it is not fine-tuned, in the sense that smoothly deforming $a_x(k)$ will move the degeneracy, but not remove it; such degeneracies can only be removed pairwise.

Since at both $\bar{\Gamma}$ and $\bar{M}$, the eigenvalues of W_k are fixed to $+1$ and -1, the parity of the number of linear crossings is a topological invariant, that cannot be changed without closing the gap in the bulk band spectrum. Returning to the possibility that $\cos|\mathbf{a}(k)|=0$ for all k: since in this case the eigenvalues of W_k are never degenerate, it trivially follows that the parity of linear in k band crossings cannot be changed without closing the bulk gap.

C. Winding of the bent Wilson loop

The product of C_{2x} and $\tilde{C}_{2,110}$ yields the screw symmetry, $\tilde{C}_4\equiv\{C_{4z}|\frac{1}{2}\frac{\bar{1}}{2}\frac{1}{2}\}$. Applying Eq (S17) with $\delta_z=\frac{1}{2}$, and removing the dagger on the righthand side of Eq (S17) because $\tilde{C}_4$ leaves k_z invariant, requires that the eigenvalues of $\mathcal{W}_{(k,k,k_{z0})}$ are exactly opposite those of $\mathcal{W}_{(-k,k,k_{z0})}$.

If there is an odd number of linear band crossings in the spectrum of $\mathcal{W}_{(k,k,k_{z0})}$ for $0\leq k\leq\pi$, then one band must

have eigenvalue $e^{i\varphi(k)}$, where $\varphi(0) = 0$ and $\varphi(\pi) = \pi$. The eigenvalue of the other band is given by $e^{i\pi - i\varphi(k)}$, according to Eq (S20). Then $\tilde{C}_4$ requires that one band of $\mathcal{W}_{(-k,k,k_{z0})}$ has eigenvalue $-e^{i\pi-i\varphi(k)} = e^{-i\varphi(k)}$; we use this band to define $\varphi(k)$ when $-\pi < k < 0$, i.e., $\varphi(-k) = -\varphi(k)$. Thus, if we plot $\varphi(k)$ from $-\pi < 0 < \pi$, it "winds" from $-\pi$ to π. This is exactly what is shown in Fig. 3b. Applying the same logic to the other band shows that it winds in the opposite direction.

S4. WILSON-OF-WILSON LOOP

Let C be the closed path in the surface Brillouin zone that traverses $\bar{\Gamma} - \bar{X} - \bar{M} - \bar{Y} - \bar{\Gamma}$ and, for each $k_\perp \in C$, let $|v_{1,2}(k_\perp)\rangle$ by the eigenstates of $\mathcal{W}_{(k_\perp,0)}$ with energies -1 and $+1$, respectively. We define the Berry phase of the Wilson loop (the "Wilson-of-Wilson" loop) by $w = e^{i \oint_C dk_\perp a(k_\perp)}$, where $a(k_\perp) = i\langle v_1(k_\perp)|\partial_{k_\perp}|v_1(k_\perp)\rangle$.

We show that the symmetry $C_{2z}\mathcal{T}$ requires $w = \pm 1$. In analogy to Eq (S20), the Wilson matrix satisfies,

$$\mathcal{W}_{(k_\perp,0)} = \tilde{U}_{C_{2z}\mathcal{T}}(k_\perp,0)K\mathcal{W}^\dagger_{(k_\perp,0)}K\tilde{U}_{C_{2z}\mathcal{T}}(k_\perp,0)^\dagger, \tag{S26}$$

where,

$$\left[\tilde{U}_{C_{2z}\mathcal{T}}(k_\perp,k_z)\right]_{nm} \equiv \langle u^n(k_\perp,-k_z)|C_{2z}\mathcal{T}|u^m(k_\perp,k_z)\rangle \tag{S27}$$

When $k_\perp \in C$, $\mathcal{W}_{(k_\perp,0)}$ is Hermitian, as we showed in Sec S3 A. Hence, $\tilde{U}_{C_{2z}\mathcal{T}}(k_\perp,0)K$ is an anti-unitary symmetry that commutes with $\mathcal{W}_{(k_\perp,0)}$ and hence does not mix the two Wilson bands, which are gapped with eigenvalues ± 1 along C. Thus, Eq (S20) can be applied with $\mathcal{W}$ replaced by w:

$$w = e^{i\phi(\bar{\Gamma})}KwKe^{-i\phi(\bar{\Gamma})} \tag{S28}$$

and

$$e^{i\phi(k_\perp)} = \langle v_1(k_\perp)|\tilde{U}_{C_{2z}\mathcal{T}}(k_\perp)|v_1(k_\perp)\rangle, \tag{S29}$$

Eq (S28) shows that w is real and equal to ± 1.

* Permanent Address: Department of Physics, Princeton University, Princeton, New Jersey 08544, USA

[1] J. C. Slater and G. F. Koster, Phys. Rev. **94**, 1498 (1954).
[2] A. Alexandradinata, X. Dai, and B. A. Bernevig, Physical Review B **89**, 155114 (2014).
[3] L. Elcoro, B. Bradlyn, Z. Wang, M. G. Vergniory, J. Cano, C. Felser, B. A. Bernevig, D. Orobengoa, G. de la Flor, and M. I. Aroyo, Journal of Applied Crystallography **50**, 1457 (2017), arXiv:1706.09272.
[4] H. C. Po, A. Vishwanath, and H. Watanabe, Nature Communications **8**, 50 (2017), arXiv:1703.00911.
[5] B. Bradlyn, L. Elcoro, J. Cano, M. G. Vergniory, Z. Wang, C. Felser, M. I. Aroyo, and B. A. Bernevig, Nature **547**, 298 (2017), arXiv:1703.02050 [cond-mat].
[6] L. Fu and C. L. Kane, Phys. Rev. B **76**, 045302 (2007).
[7] M. I. Aroyo, ed., *International Tables for Crystallography*, Vol. A (International Union of Crystallography, 2016).
[8] M. I. Aroyo, A. Kirov, C. Capillas, J. M. Perez-Mato, and H. Wondratschek, Acta Cryst. **A62**, 115 (2006).
[9] S. Altmann and P. Herzig, *Point-Group Theory Tables*, 2nd ed. (University of Vienna, 2011).
[10] M. I. Aroyo, J. M. Perez-Mato, D. Orobengoa, E. Tasci, G. de la Flor, and A. Kirov, Bulg. Chem. Commun. **43(2)**, 183 (2011).
[11] A. Alexandradinata, Z. Wang, and B. A. Bernevig, Phys. Rev. X **6**, 021008 (2016).
[12] B. J. Wieder, B. Bradlyn, Z. Wang, J. Cano, Y. Kim, H.-S. D. Kim, A. M. Rappe, C. L. Kane, and B. A. Bernevig, (2017), arXiv:1705.01617.